Empirical model of lower band chorus wave distribution in the outer radiation belt

V S Agapitov, V S Artemyev, D. Mourenas, F S Mozer, V S Krasnoselskikh

AGU PUBLICATIONS

JGR

Journal of Geophysical Research: Space Physics

RESEARCH ARTICLE

10.1002/2015JA021829

Key Points:
- The model for chorus wave amplitude and obliqueness is presented
- Input parameters for the model are *Kp* index, geomagnetic latitude, MLT, and *L* shell
- The model can be directly applied for diffusion rates calculation

Supporting Information:
- Text S1 and Caption for Figure S1
- Figure S1

Correspondence to:
O. V. Agapitov,
oleksiy.agapitov@gmail.com

Citation:
Agapitov, O. V., A. V. Artemyev, D. Mourenas, F. S. Mozer, and V. Krasnoselskikh (2015), Empirical model of lower band chorus wave distribution in the outer radiation belt, *J. Geophys. Res. Space Physics*, *120*, 10,425–10,442, doi:10.1002/2015JA021829.

Received 19 AUG 2015
Accepted 23 NOV 2015
Accepted article online 27 NOV 2015
Published online 17 DEC 2015
Corrected 2 NOV 2016

This article was corrected on 2 NOV 2016. See the end of the full text for details.

Empirical model of lower band chorus wave distribution in the outer radiation belt

O. V. Agapitov[1,2], A. V. Artemyev[3,4], D. Mourenas[5], F. S. Mozer[1], and V. Krasnoselskikh[5]

[1]Space Sciences Laboratory, University of California, Berkeley, California, USA, [2]National Taras Shevchenko University of Kiev, Kiev, Ukraine, [3]Department of Earth, Planetary, and Space Sciences and Institute of Geophysics and Planetary Physics, University of California, Los Angeles, California, USA, [4]Space Research Institute, RAS, Moscow, Russia, [5]LPC2E/CNRS, University of Orleans, Orleans, France

Abstract Accurate modeling of wave-particle interactions in the radiation belts requires detailed information on wave amplitudes and wave-normal angular distributions over *L* shells, magnetic latitudes, magnetic local times, and for various geomagnetic activity conditions. In this work, we develop a new and comprehensive parametric model of VLF chorus waves amplitudes and obliqueness in the outer radiation belt using statistics of VLF measurements performed in the chorus frequency range during 10 years (2001–2010) aboard the Cluster spacecraft. We used data from the Spatio-Temporal Analysis of Field Fluctuations-Spectrum Analyzer experiment, which spans a total frequency range from 8 Hz to 4 kHz. The statistical model is presented in the form of an analytical function of latitude and *Kp* (or *Dst*) index for day and night sectors of the magnetosphere and for two ranges of *L* shells above the plasmapause, from $L = 4$ to 5 and from $L = 5$ to 7. This model can be directly applied for numerical calculations of charged particle pitch angle and energy diffusion coefficients in the outer radiation belt, allowing to study with unprecedented detail their statistical properties as well as their important spatiotemporal variations with geomagnetic activity.

1. Introduction

One of the major tasks for the geophysics community is to develop full-scale radiation belt codes aiming at forecasting the risks for the myriads of satellites in service, since relativistic flux variations are often leading to malfunctions, and unexpected failures of electronics [*Horne et al.*, 2013]. Besides models based on linear/nonlinear correlation analysis of spacecraft data [*Balikhin et al.*, 2011; *Kellerman et al.*, 2013; *Boynton et al.*, 2013], physics-based models are widely used for the description of the evolution of high-energy electron fluxes in the radiation belts (see review *Shprits et al.* [2008], and references therein). One basic element of such models is the underlying assumption that the evolution of wave-particle resonant interactions can be well described in the framework of quasi-linear theory [*Trakhtengerts*, 1966; *Kennel and Petschek*, 1966]. This theory assumes that average wave amplitudes are small enough and the wave spectrum wide enough (over multiple bounce periods) to consider wave-particle resonant interactions as a random process characterized by a relatively slow scattering of particles in velocity space. A convenient approach corresponds to the calculation of particle pitch angle and energy diffusion coefficients and their subsequent incorporation into the Fokker-Plank equation [*Lyons and Williams*, 1984]. There are several well-developed codes that allow calculating such diffusion coefficients under various approximations [*Glauert and Horne*, 2005; *Summers*, 2005; *Shprits et al.*, 2006; *Albert*, 2007, 2008] as well as analytically [*Mourenas and Ripoll*, 2012; *Mourenas et al.*, 2012]. All these schemes rely on several models concerning the background magnetospheric environment and the main properties of the wave spectrum. Besides magnetic field models [e.g., *Tsyganenko et al.*, 2003] and statistical background plasma density models [e.g., *Sheeley et al.*, 2001; *Ozhogin et al.*, 2012] two different and complementary types of wave models are needed.

1. A model giving the distribution of the wave magnetic field amplitude. The wave intensity B_w^2 recorded onboard satellites strongly depends on the wave frequency range, *L* shell, magnetic latitude, magnetic local time (MLT), and geomagnetic activity. Typically, ELF/VLF waves in the radiation belts may be separated by their frequency ω to local equatorial electron gyrofrequency Ω_{ce0} ratio as upper band chorus waves with $0.5\Omega_{ce0} < \omega < \Omega_{ce0}$, lower band chorus waves with $0.1\Omega_{ce0} < \omega < 0.5\Omega_{ce0}$, hiss waves with $\Omega_{LH} < \omega < 0.1\Omega_{ce0}$ and a possible extension below $\Omega_{LH} \sim (m_e/m_i)^{1/2}\Omega_{ce0}$ [*Meredith et al.*, 2004; *Li et al.*, 2013a], fast magnetosonic waves with $m_e/m_i\Omega_{ce0} < \omega < \Omega_{LH}$ (where m_e/m_i is the ratio of the electron mass to the effective mass of ions), and ULF electromagnetic ion cyclotron waves with ω around of gyrofrequencies

of oxygen, helium, and hydrogen. These different wave populations are generally present in different regions of the radiation belts and have different intensities [*Meredith et al.*, 2001, 2004, 2012, 2014; *Agapitov et al.*, 2013; *Mourenas et al.*, 2013]. In the outer radiation belt (above the plasmapause), lower band chorus waves are generally the most intense emissions. They are probably responsible for some of the most efficient wave-particle interactions in the outer radiation belt [*Thorne et al.*, 2013]. Chorus waves are right-hand polarized coherent waves, characterized by discrete structures in frequency-time diagrams [see, e.g., *Helliwell*, 1965; *Agapitov et al.*, 2011a, 2010, and reference therein]. These emissions are observed predominantly near and outside the outer boundary of the plasmasphere [*Koons and Roeder*, 1990; *Tsurutani and Smith*, 1974; *Sazhin and Hayakawa*, 1992; *Gurnett and Inan*, 1988]. Chorus waves occur typically from 00:00 to 15:00 MLT, with a peak between 06:00 and 12:00 MLTs [*Koons and Roeder*, 1990; *Tsurutani and Smith*, 1974]. Recently, several statistical models of wave distributions have been proposed by making use of wave measurements obtained on board of the Dynamics Explorer 1 [*André et al.*, 2002], CRRES [*Meredith et al.*, 2001, 2004], Cluster [*Pokhotelov et al.*, 2008; *Agapitov et al.*, 2011c, 2012], and Thermal Emission Imaging System (THEMIS) [*Cully et al.*, 2008; *Li et al.*, 2011] spacecraft. For fixed geomagnetically activity level, the wave intensity distribution can be roughly characterized by two MLT domains (wherein the wave amplitude distribution remains similar based on Kolmogorov-Smirnov statistical analysis): dayside (or dawnside/dayside—from 3:00 to 15:00 MLT) and nightside (or nightside/duskside—from 15:00 to 3:00 MLT). Moreover, each MLT domain may also be roughly separated into two L shell regions: $L \in [4, 5\text{-}5.5]$ and $L \in [5-5.5, 9]$ [*Agapitov et al.*, 2013; *Mourenas et al.*, 2014]. In each of these four subregions, the wave intensity depends on latitude λ [*Meredith et al.*, 2012; *Bunch et al.*, 2012; *Agapitov et al.*, 2013]. This dependence was approximated in many studies by different models: stepwise functions were used by *Horne et al.* [2005b] and *Ni et al.* [2011], polynomial fitting up to $|\lambda| < 15°$ was provided by *Spasojevic and Shprits* [2013], and a polynomial fitting over a wide λ range for several fixed levels of geomagnetic activity was described by *Artemyev et al.* [2012b] and *Mourenas et al.* [2014]. However, at this date, a unique approximation providing the wave intensity as a function of latitude and geomagnetic activity over the whole latitude range $|\lambda| < 45°$ (most lower band chorus waves cannot penetrate to higher latitudes due to their reflection when their frequency reaches the lower hybrid frequency) is still lacking.

2. The distribution of wave-normal angles. Besides its intensity, each wave is also characterized by the angle θ between its direction of propagation and the background magnetic field. The distribution of chorus wave-normal angles $g(\theta)$ has been a subject of interest and debates during the past few decades, but it has mainly been studied in the vicinity of the equator [*Hayakawa et al.*, 1984; *Lauben et al.*, 2002; *Goldstein and Tsurutani*, 1984; *Burton and Holzer*, 1974], where values of θ have generally been estimated as less than 30°. *Burton and Holzer* [1974] found that of lower band chorus, θ was less than 30° for 80% of the events at $|\lambda| < 40°$ and that it extended to ~85° for $|\lambda| > 40$ with a spreading of the distribution of θ. A similar behavior was found by *Haque et al.* [2010] for upper band chorus on the basis of Polar measurements, but the direction of propagation was found to be closer to the background magnetic field for lower band chorus waves. A statistics of whistler wave-normal directions was presented by *Agapitov et al.* [2011b] for $|\lambda| < 30°$. The distribution $g(\theta)$ was shown to depend on local coordinates (L shell, MLT, and latitude) and on geomagnetic activity. There are two main processes responsible for the formation of the $g(\theta)$ distribution of chorus waves: wave spreading in the course of its propagation in the inhomogeneous magnetic field of the Earth's dipole [e.g., *Shklyar et al.*, 2004; *Breuillard et al.*, 2012, and references therein] and Landau damping of highly oblique whistler mode waves [*Bortnik et al.*, 2006; *Chen et al.*, 2013]. The competition between these two processes results in the observed variation of the $g(\theta)$ distribution with latitude, MLT, L shell, and geomagnetic activity. Although parallel (or quasi-parallel) wave propagation $\theta \approx 0$ is often considered in many modern models of quasi-linear diffusion by whistler mode waves [*Glauert and Horne*, 2005; *Shprits et al.*, 2006; *Summers et al.*, 2007; *Albert*, 2007], it has also been shown that a finite (>45°) value of the mean θ angle could play a potentially important role for electron resonant scattering [*Shprits and Ni*, 2009; *Artemyev et al.*, 2012a; *Albert*, 2012; *Ni et al.*, 2013; *Glauert et al.*, 2014; *Li et al.*, 2014]. Recent spacecraft observations have revealed the existence of a subpopulation of whistler mode waves with very oblique $\theta \in [\theta_g, \theta_r]$ [*Li et al.*, 2011; *Agapitov et al.*, 2012], where θ_g and θ_r are the Gendrin and resonance cone angles [*Gendrin*, 1961]. The mean intensity of magnetic field fluctuations associated with such very oblique waves is substantially smaller than that for parallel waves on average [*Santolík et al.*, 2014], but their impact on electron resonant scattering can remain significant during quiet to moderately disturbed geomagnetic conditions [*Artemyev et al.*, 2013a; *Mourenas et al.*, 2014; *Li et al.*, 2014]. The $g(\theta)$ distribution derived from Cluster spacecraft observations has been approximated as a function of latitude for three geomagnetic activity ranges in the works

by *Artemyev et al.* [2013a] and *Mourenas et al.* [2014]. However, a continuous representation $g(\theta) = f(Kp)$ as a function of geomagnetic activity is still lacking, which is an important restriction for anyone aiming at accurately simulating the full spatiotemporal dynamics of the radiation belts.

Quasi-linear diffusion coefficients depend also on the wave frequency distribution [*Lyons and Williams*, 1984]. Spacecraft observations suggest that the spectrum of lower band chorus waves has a maximum power around $\omega/\Omega_{ce0} = \omega_m/\Omega_{ce0} \sim 0.3$ and a Gaussian distribution around this maximum with $\Delta\omega \sim 0.15\Omega_{ce0}$ at low to moderate latitudes [*Meredith et al.*, 2003b]. The variation of ω_m with latitude has been considered by *Bunch et al.* [2013] and *Breuillard et al.* [2015], and it was found to have a relatively weak effect on wave-particle resonant interactions, at least for electron energies $E < 2$ MeV [*Breuillard et al.*, 2015]. In the two above models of wave intensity and θ distributions, the dependence on geomagnetic activity can be determined using various geomagnetic indices: *AE*, *Kp*, *Dst*, or solar wind parameters (IMF, solar wind velocity, and density). For example, detailed and comprehensive statistics from CRRES have been used to provide models of wave intensity as a function of *AE* [*Meredith et al.*, 2001, 2003b] and *Kp* [*Shprits et al.*, 2007; *Spasojevic and Shprits*, 2013]. Cluster statistics for both the wave intensity and $g(\theta)$ distributions have also been fitted for a few separate ranges of *Kp* [*Agapitov et al.*, 2013] and *Dst* [*Artemyev et al.*, 2013a; *Mourenas et al.*, 2014]. In several other studies, the solar wind conditions have been considered as the main parameters governing the wave intensity variation [*Bunch et al.*, 2012; *Kim et al.*, 2013].

As a matter of fact, space weather models of the radiation belts are often making use of only one parameterization of the wave characteristics, for instance, as a function of either *Kp* or *Dst*. By doing so, it is implicitly assumed that all these indices correlate sufficiently well with each other, so that using only one of them should be sufficient. It is true that some level of correlation often exists. Various studies have demonstrated the existence of rough relationships between *Dst* and *Kp* (over ~3 h) [*Yermolaev and Yermolaev*, 2003], between *Dst* and solar wind conditions [*Nikolaeva et al.*, 2013], or between *AE* and solar wind conditions [*Nikolaeva et al.*, 2011]. However, it is also well known that there is no unique relationship between each two of these parameters (*AE*, *Kp*, *Dst*, and solar wind conditions). The different indices correspond to different kinds of measurements and probably describe with different weights the various physical processes leading to the presence of the waves. For example, the quasi-logarithmic *Kp* index measures the maximum range of any component of the geomagnetic field intensity seen at midlatitudes, while the *Dst* index ideally measures the ring current magnetic field, based on averages of the disturbances of the horizontal field component recorded at low-latitude observatories [*Mayaud*, 1980]. The *AE* index measures primarily variations in the auroral electrojets by providing the fluctuations of the horizontal component of the field from auroral zone laboratories. Thus, all these indices are at least partially independent [e.g., see *Gonzalez et al.*, 1994; *Huttunen et al.*, 2002] and may provide useful, complementary information on the wave distributions.

In this paper, we first present the general expression of quasi-linear diffusion coefficients to show how and under what form the main characteristics of the waves (amplitude and wave-normal distributions) will be taken into account. Then, we analyze Cluster data recorded between 2001 and 2010 [*Agapitov et al.*, 2011b, 2012] to derive new and more comprehensive empirical models of chorus wave distribution as a function of magnetic latitude λ and L shell for different levels of geomagnetic activity (represented by *Kp* and *Dst* indices) in the region $|\lambda| < 40°$ at radial distances from 4 up to 7 R_E. The models for the wave-normal angle and wave magnetic field amplitude can be directly used for calculating numerically the corresponding quasi-linear diffusion coefficients, as demonstrated in the last section of this paper. These preliminary results reveal strong and complex variations of scattering with geomagnetic activity, as well as interesting differences between results obtained with wave models relying on *Kp* or *Dst*.

In two previous papers, some preliminary models of the wave magnetic field ($\langle B_w^2 \rangle$) and θ distributions have already been provided as a function of *Dst* on the basis of Cluster data [*Artemyev et al.*, 2013b; *Mourenas et al.*, 2014]. However, these previous models were restricted to only three *Dst* ranges, seriously limiting their usefulness in practice. Here we present a more comprehensive chorus wave model characterized by a continuous dependence of both $\langle B_w^2 \rangle$ and $g(\theta)$ on *Dst* for day and night sectors, as well as an entirely new and complementary model giving $\langle B_w^2 \rangle$ and $g(\theta)$ as a continuous function of *Kp*. These two models are written under the form of polynomial functions, therefore allowing a smooth dependence on both geomagnetic activity and magnetic latitude. Moreover, such a continuous representation has an additional implicit advantage: due to the weight of neighboring points in the polynomial fit, it contains a somewhat natural interpolation (or sometimes extrapolation) between parameter regions with full data coverage (i.e., with more than 100

measurements per separate bin) when one encounters a small parameter domain with more sparse data. In the last section, the wave models are used to calculate numerically the corresponding quasi-linear diffusion coefficients. Preliminary results demonstrate the strong variations of scattering with geomagnetic activity as well as interesting differences between results obtained with wave models relying on *Kp* (or *Dst*).

2. Description of Wave and Plasma Parameters Required for the Calculation of Quasi-Linear Diffusion Rates

The general form of pitch angle diffusion coefficients for electrons resonantly interacting with whistler mode waves can be written as [*Glauert and Horne*, 2005]

$$D_{\alpha\alpha} = \frac{e^2}{4\pi}\sum_n \int_{\theta_{\min}}^{\theta_{\max}} \frac{d\theta}{\cos\theta} \sum_i \frac{\hat{B_w^2}(\omega_i)\sin\theta\tilde{g}(\theta)\left|\Phi_{n,k}\right|^2}{N(\omega_i)\left|v_\parallel - \partial\omega/\partial k_\parallel\right|_{k_{\parallel i}}} \times \left(\frac{n\Omega_{ce}/\gamma - \omega_i \sin^2\alpha}{\cos\alpha}\right)^2 \quad (1)$$

where n is the harmonic number, i is the number of the resonant root, $\theta_{\min}$ and $\theta_{\max}$ are limits determined by the model used ($\theta_{\min} = 0$ and $\theta_{\max}$ is slightly below the resonance cone θ_{res}—see details in *Artemyev et al.*[2013b]), and ω_i, k_i are solutions of equations

$$\omega = \omega(k,\theta)$$
$$\omega - k_\parallel v_\parallel = -n\Omega_{ce}/\gamma$$

$\omega = \omega(k,\theta)$ is the dispersion relation, α is the particle pitch angle, $v_\parallel = \sqrt{1-\gamma^{-2}}\cos\alpha$, and γ is the relativistic factor. The function $\Phi_{n,k}$ describes the relation between the wave electric and magnetic field components [*Glauert and Horne*, 2005]. All local system parameters (for given λ) are included into functions $G(\theta) = \sin\theta\tilde{g}(\theta)/N(\omega_i)$ and $\hat{B_w^2}$. The latter defines the spectral distribution of wave intensity evaluated at the resonant root ω_i

$$\hat{B_w^2}(\omega_i) = A\exp\left(-\frac{(\omega_m - \omega_i)^2}{\delta\omega^2}\right) \quad (2)$$

where A is the normalization constant, $\int_{\omega_{\min}}^{\omega_{\max}} \hat{B_w^2}(\omega)d\omega = B_w^2$, and $B_w^2(\lambda)$ is the local wave intensity. The function $G(\theta)$ gives the normalized distribution of wave magnetic energy as a function of θ at a given latitude

$$G(\theta) = 2\pi^2 \sin\theta\tilde{g}(\theta)\left(\int_{\theta_{\min}}^{\theta_{\max}} \sin\theta\tilde{g}(\theta)k^2 \left.\frac{\partial k}{\partial\omega}\right|_\theta d\theta\right)^{-1}$$

where $\tilde{g}(\theta)$ is the probability distribution function (PDF) at angle θ. This function determines the amount of wave energy with a wave-normal angle θ in the element of $\mathbf{k}^3$ space $dk^2 = \sin\theta k^2 dk d\theta$. Spacecraft measurements provide the amount of waves in the elementary volume $k^2 dk d\theta$. Thus, measurements already provide the function $g(\theta) = \tilde{g}(\theta)\sin\theta$. This function $g(\theta)$ can be approximated by two Gaussians [*Artemyev et al.*, 2013a; *Mourenas et al.*, 2014]

$$g(\theta) = \exp\left(-\frac{(\theta-\theta_1)^2}{\delta\theta_1^2}\right) + Q^2\exp\left(-\frac{(\theta-\theta_2)^2}{\delta\theta_2^2}\right) \quad (3)$$

where the factor Q depends on *Kp* (or *Dst*), on L shell, as well as on geomagnetic latitude and MLT. Parameters $\theta_1, \theta_2, \delta\theta_1 \approx \delta\theta_2$ are almost the same for dayside and nightside and do not depend strongly on L shell either. These parameters can be approximated by polynomials as a function of latitude

$$\theta_j = \sum_{i=0}^{5} a_{ji}(\lambda/10°)^i$$
$$\delta\theta_j = \sum_{i=0}^{5} b_{ji}(\lambda/10°)^i \quad (4)$$

Table 1. Values of the Coefficients a_{ji} and b_{ji} Used for Approximations of $\theta_{1,2}$ and $\delta\theta_{1,2}$

i	a_{1i}	a_{2i}	$b_{(1,2)i}$
0	11.54	66.0	5.68
1	14.32	1.0	4.62
2	−8.18	0.0	3.05
3	1.22	0.0	−5.06
4	0.0	0.0	1.83
5	0.0	0.0	−0.203

where coefficients a_{ji} and b_{ji} are given in Table 1. Figure 1 based on Cluster statistics shows that θ_1, θ_2, $\delta\theta_1$, and $\delta\theta_2$ vary rather weakly with latitude. Reasonable approximations for these functions are $\theta_1 \approx 15°$, $\theta_2 \approx 70°$, and $\delta\theta_{1,2} \approx 10°$. The nearly constant value of these parameters can be explained in the following way: almost all the variations of the θ distribution with latitude correspond to the factor Q in equation (3), while the two exponents in $g(\theta)$ are almost independent of the system parameters. Physically, it could be related to the preferential generation of whistler mode waves with small θ values at low latitudes and their later convergence during their propagation to higher latitudes toward the θ range comprised between the Gendrin angle and the resonance cone angle [*Chen et al.*, 2013; *Breuillard et al.*, 2012]. In such a situation, the variation of the number of oblique waves with latitude, geomagnetic activity, and L shell should be mainly controlled by the Q factor alone.

Besides, a model of equatorial plasma density N_e is also needed. In the trough, one may use $N_e \sim 100\,(4/L)^4$ cm^{-3} which is close to the average value obtained from CRRES data in the region $4 < L < 7$ (see the leading term in equation (7) from *Sheeley et al.* [2001]). The variation of N_e along magnetic field lines can be further approximated as $N_e(\lambda)/N_e(\lambda = 0) \sim \cos^{-5}(\lambda)$ [*Denton et al.*, 2006]. Note that the average trough density was found to be relatively weakly varying with geomagnetic activity for $0 < Kp < 5.5$ on the basis of CRRES results [*Sheeley et al.*, 2001], although strong variations are possible during given events. A comparison of existing plasma density models and a detailed discussion of the latitudinal variation can be found in *Ozhogin et al.* [2012].

3. Data and Methods

For this work, we have utilized a large data set of VLF waves measured by the Cluster satellite between February 2001 and December 2010 over a wide domain of the inner magnetosphere, including the location of the outer radiation belt (i.e., confined to $|\lambda| < 45°$ and $4 \le L \le 7$). This region is thought to be of primary importance for the generation of chorus waves and the related processes of electron energization and loss. To determine the properties of the wave amplitude and normal angle distributions (see *Agapitov et al.* [2013] for details), we have used the data from the Spatio-Temporal Analysis of Field Fluctuations-Spectrum Analyzer (STAFF-SA) experiment [*Cornilleau-Wehrlin et al.*, 2003], which provides the complete spectral matrix (the real and the imaginary part) of the three magnetic components as measured by the STAFF search coil

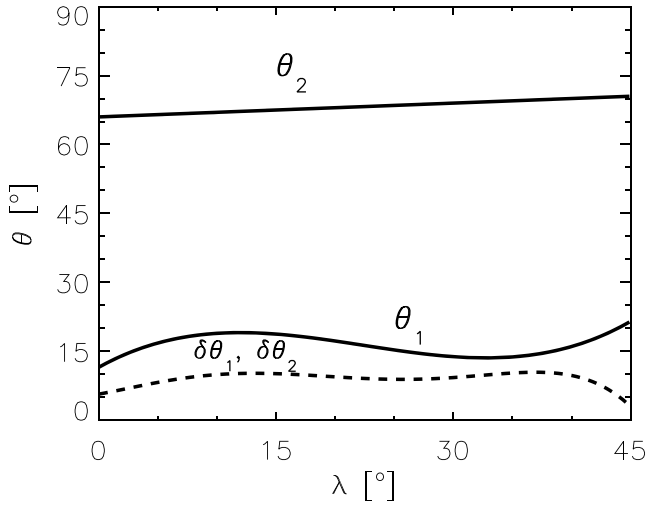

Figure 1. θ_1, θ_2, and $\delta\theta_{1,2}$ as functions of latitude.

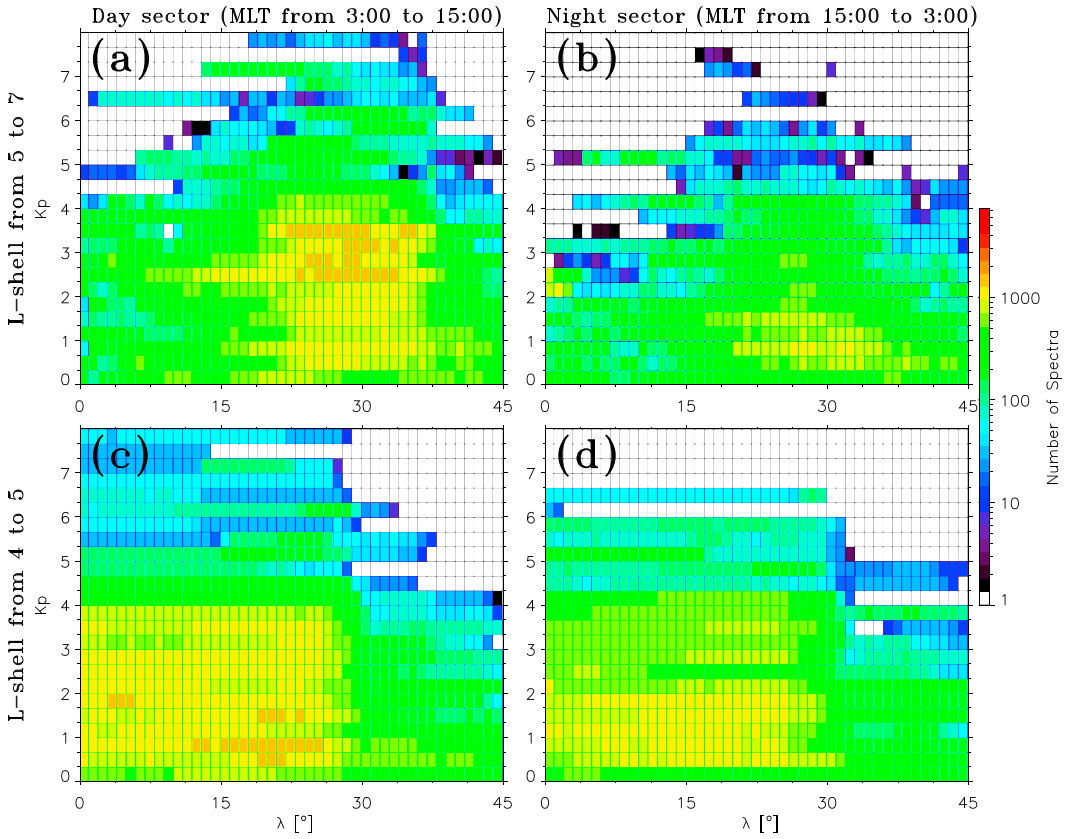

Figure 2. Data coverage of the Cluster STAFF-SA measurements during 2001–2010 in the chorus frequency range ($0.1\Omega_{ce} < \omega < \Omega_{ce}$) as a number of spectra captured in a magnetic latitude λ *Kp* domain for day/night sector and two *L* shell ranges: from 4 to 5 and from 5 to 7.

magnetometer and the two electric field components captured by electric fields and wave experiment [*Gustafsson et al.*, 2001].

Our survey only includes STAFF-SA data from the single Cluster 4 spacecraft (Samba) in order to avoid redundant statistical contributions and biases due to different cross-spacecraft distances during the processing period. The analyzed wave frequency range includes electron whistler mode waves from $\omega \sim 0.1\Omega_{ce}$ to Ω_{ce}. This range is known to be dominated by chorus waves in two frequency bands below and above $0.5\Omega_{ce}$: lower band and upper band chorus, respectively [*Burtis and Helliwell*, 1976]. Here we shall focus on the former frequency range and consider only waves outside the plasmasphere (see details below), corresponding most generally to lower band chorus.

Our analysis relied on spectral matrices computed on board the Cluster spacecraft for 27 frequency channels with central frequencies logarithmically spaced between 8.8 Hz and 3.56 kHz covering the frequency range from 8 Hz to 4 kHz. The sensitivity of the STAFF search coil magnetometers was $5 \cdot 10^{-3}$ nT Hz$^{-1/2}$ at 1 Hz and $4 \cdot 10^{-5}$ nT Hz$^{-1/2}$ at 100 Hz and 4 kHz [*Cornilleau-Wehrlin et al.*, 2003]. We excluded measurements with amplitudes below twice the STAFF-SA sensitivity level from wave-normal processing while taking these low-level signals into account for the wave amplitude analysis.

The Cluster data set contains a sufficient number of points for performing a statistical study over the considered range of magnetic local times (MLTs) and *L* shells, as illustrated in Figure 2. For low geomagnetic activity ($Kp \leq 3$), the coverage is very good with only relatively poorer measurements near the equator at $L > 5$ and $-10° < \lambda < 0°$. For intermediate geomagnetic activity ($Kp = 3$ to 5.5), the coverage is still good enough for $4 < L < 7$ at all latitudes $|\lambda| < 45°$. For very high geomagnetic activity ($Kp = 6$–8), the coverage remains acceptable at $|\lambda| < 35°$for $4 < L < 5$, at $5° < |\lambda| < 40°$ on the dayside for $L = 5$–7, and at $5° < |\lambda| < 35°$ in the night sector at $L = 5$–7 only when $Kp < 7$.

To develop a comprehensive empirical model of wave activity, the following parameters have been used: (1) the location of the wave occurrences (i.e., L shell, MLT, and λ), (2) the wave characteristics (magnitude of the wave magnetic field component and wave vector direction relative to the background magnetic field), and (3) the geomagnetic activity conditions as characterized by the Kp index (the complementary Dst index model is provided in the Appendix). On this basis, polynomial models of RMS wave amplitude and wave obliquity factor Q (characterizing the relative amount of oblique magnetic wave power) have been derived making use of root-mean-square fitting techniques. Such a smooth, continuous modeling as a function of parameters allows to provide reasonable estimates even inside limited parameter ranges where satellite coverage is less good, thanks to the weighted contribution from neighboring domains to the overall fitting.

Note also that the first L sector has been defined from $L = 4$ (or from the plasmapause position if it is at higher L; plasmapause position with dependence on MLT is estimated from the model by *Doe et al.* [1992]) to $L = 5$ for two reasons. First, the behavior of the waves changes in observations between $L \leq 5-5.5$ and $L > 5-5.5$. Second, as that the maximum frequency of the STAFF instrument is 4 kHz, the mean lower band chorus frequency $\sim 0.3-0.35\, f_{ce}$ goes above the instrument passband for $L < 4$, which would lead to a serious underestimation of lower band chorus power (between ~ 0.1 and $\sim 0.45 f_{ce}$) at lower Ls. Between $L = 4$ and 4.5, the spectrum power should not be underestimated by more than a factor of 2 (mostly less when taking into account the orbit of Cluster), and this underestimation disappears at $L > 4.5$. For $4 < L < 4.5$ a correction factor based on the assumption of a Gaussian distribution of wave power (with a maximum at $f = 0.3 f_{ce}$ and a variance $\Delta f = 0.15 f_{ce}$) was used to recover the full wave power. Since all the available measurements between $L = 4$ and $L = 5$ are used together to determine wave characteristics inside this first L sector, average (RMS) wave characteristics such as the lower band chorus wave power should remain roughly accurate over this sector.

4. Model of Wave Amplitudes $B_w(\lambda)$ as a Function of Kp

The present parameterized model of lower band chorus wave amplitude in the magnetosphere includes three individual components representing the dependence on θ, λ, and L shell, respectively, in the day and night sectors and for different geomagnetic activity regimes defined by the Kp index. The distribution of root-mean-square (RMS) wave amplitude B_w in the λ Kp domain is displayed in Figure 3 over the full range of filled cells. The statistical measured dependence is well reproduced by third-order polynomial fits as a function of λ and Kp

$$\log_{10} B_w(\lambda, K_p)[\mathrm{nT}] = \sum \sum a_{ij} (K_p)^j (\lambda[^\circ]/10)^i, \tag{5}$$

The values of the different coefficients a_{ij} are provided in Table 2.

A local minimum of B_w in the vicinity of the equator can be seen in Cluster statistics for all Kp in the day sector, as well as for $Kp < 5$ in the night sector. It is well reproduced by the model. Model values of B_w are indicated in Figure 3 by contour lines with colors corresponding to B_w magnitude, allowing a rough comparison. Moreover, precise comparisons between model and data at $L = 4-5$ for different values of the Kp index have been performed (see supporting information), demonstrating the good overall agreement: the distribution of errors is centered around zero (for the night sector shifted from zero to about 8%), and more than 60% of Cluster data points have deviation less than 20% (a similar agreement is found for $L = 5-7$). The maximum in amplitudes at $\lambda \sim 25°$ on the dayside could stem from quasi-linear wave growth due to a steepened downward electron phase space density gradient toward the loss cone in the presence of increased losses induced by oblique waves [*Mourenas et al.*, 2014]. The smaller number of collected measurements at high λ leads to some level of uncertainty there, but the decrease of B_w at $\lambda > 30°$ is nevertheless clear and real. In the night sector, the maximum of B_w observed in the vicinity of the equator during high geomagnetic activity (in agreement with previous studies [*Horne et al.*, 2005a; *Agapitov et al.*, 2013]) is also well reproduced by the proposed model. However, sparse measurements for $Kp > 6+$ (see Figure 2) limit the reliability and applicability of the model in this upper activity range.

5. Model of Wave Obliquity Q on Kp

Chorus waves are generally assumed to be generated in the close vicinity of the magnetic equator with wave-normal angles close to the background magnetic field direction [*Lauben et al.*, 2002; *Parrot et al.*, 2003]. This assumption has been confirmed in the recent works by *Agapitov et al.* [2011b, 2012] by processing the

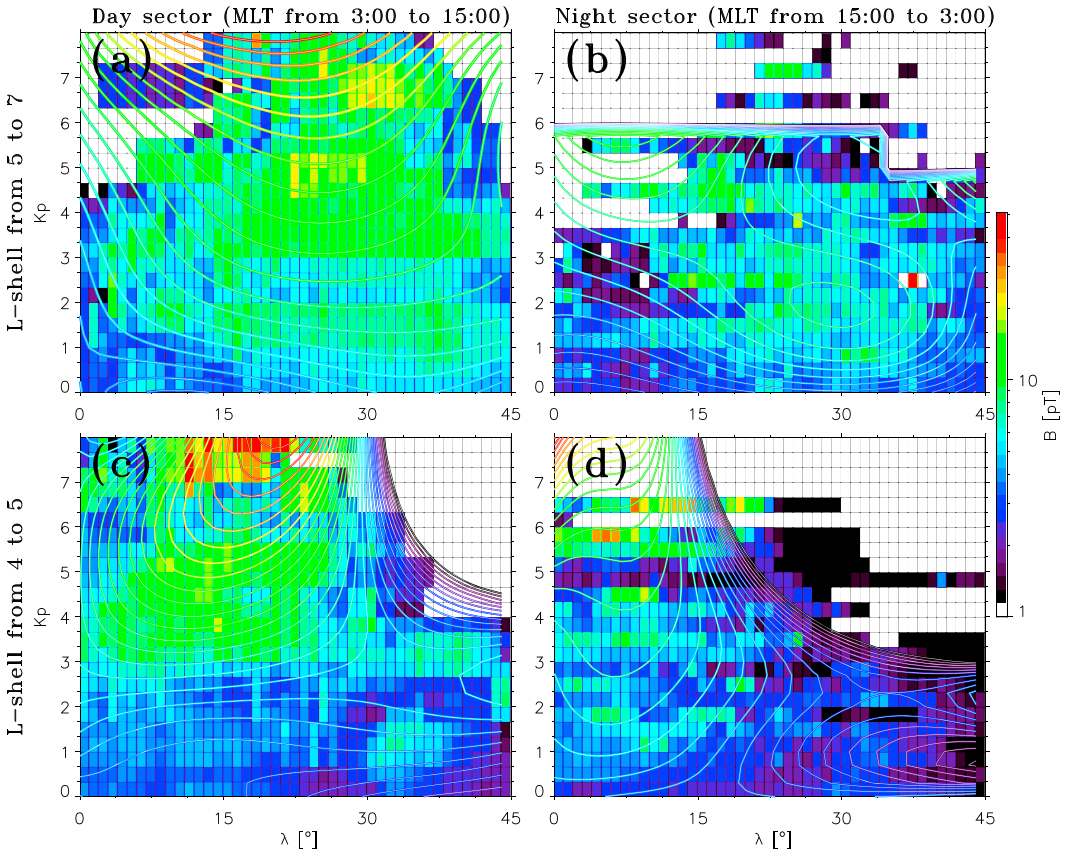

Figure 3. RMS values of lower band chorus wave amplitudes in the λ *Kp* domain for the day and night sectors of the magnetosphere for *L* shell from 4 to 5. The values obtained from Cluster measurements are shown by color of the filled cells. The model values are shown by contour lines with amplitude levels indicated by colors.

Table 2. Values of the Coefficients α_{ij} for the Model of Chorus Wave RMS Amplitude B_w (Day/Night Sectors; $4 < L < 5$ and $5 < L < 7$)

Sector	*ij*	0	1	2	3
			$4 < L < 5$		
Day	0	−2.53242	0.14836	−0.01648	0.00016
	1	0.11290	−0.47100	0.23260	−0.02317
	2	−0.08181	0.28823	−0.15163	0.01726
	3	0.01027	−0.04109	0.02380	−0.00311
Night	0	−2.39346	0.10988	−0.03083	0.00431
	1	−0.03083	0.16417	−0.01875	−0.00346
	2	−0.00884	−0.13052	0.00501	0.00680
	3	0.00334	0.00089	0.01714	−0.00523
			$5 < L < 7$		
Day	0	−2.40708	−0.02297	0.01223	−0.00021
	1	−0.29267	0.45874	−0.10822	0.00812
	2	0.18808	−0.22663	0.05810	−0.00446
	3	−0.02839	0.03140	−0.00859	0.00066
Night	0	−2.69548	0.22568	−0.04232	0.00423
	1	−0.00652	−0.09346	0.05615	−0.00424
	2	0.07774	0.12785	−0.06845	0.00524
	3	−0.01756	−0.02291	0.01166	−0.00080

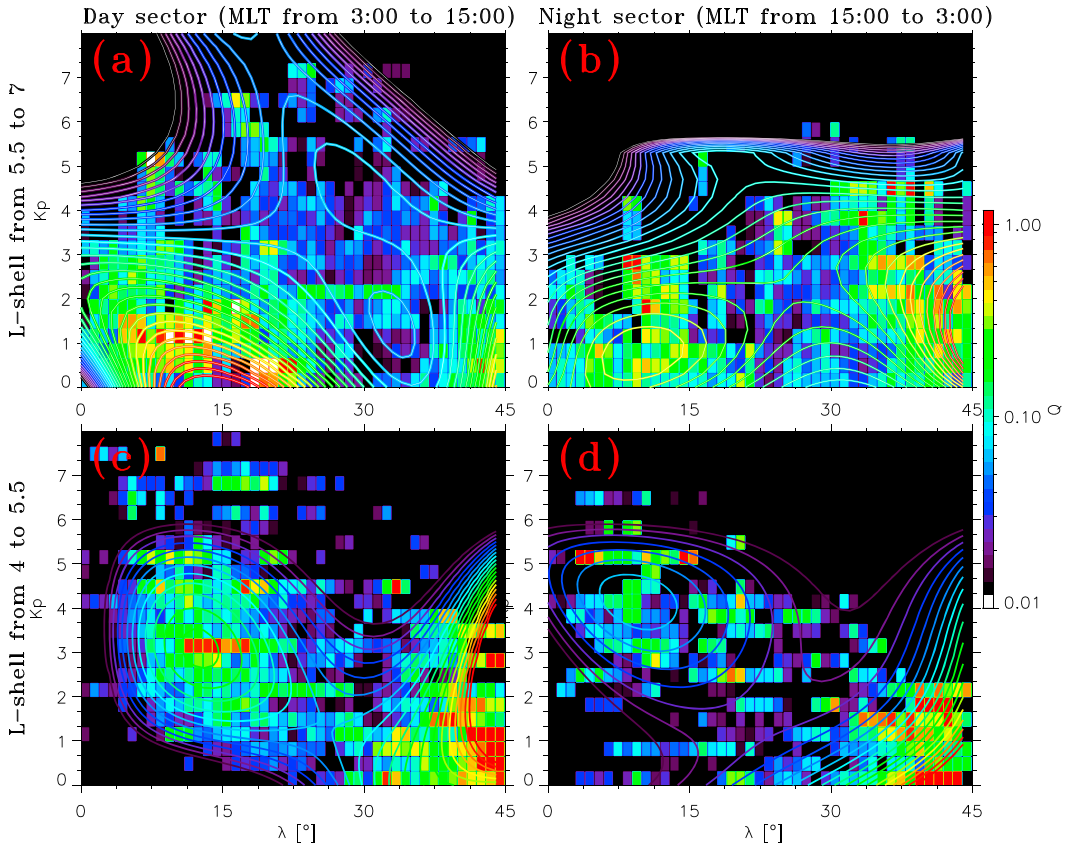

Figure 4. Distribution of the obliqueness parameter Q for chorus waves in the day and night sectors of the outer radiation belt: $4 < L < 5$ and $5 < L < 7$.

direction of the Poynting vector from the Cluster STAFF-SA spectral matrices measurements, and it was also confirmed on the basis of THEMIS statistics [*Li et al.*, 2013b]. The analysis of the probability distribution function (PDF) of the wave-normal angles θ of lower band chorus waves as a function of λ for $4 < L < 7$ has demonstrated that this distribution was significantly different from a simple Gaussian [*Agapitov et al.*, 2013; *Li et al.*, 2013b]. The actual θ distribution is nonsymmetric and its width increases with λ (especially for $L < 5.5$). This distribution may be divided into two groups of waves: nearly field aligned and oblique, with wave normals showing a clear tendency to deviate more and more from the magnetic field direction as $|\lambda|$ increases from 0°to ~25°. At $\lambda \sim 30°$, the two peaks of the θ distribution apparently merge together, forming a common distribution with a peak at approximately 70–80° and an angular spread of the same order [*Agapitov et al.*, 2013; *Artemyev et al.*, 2013a; *Mourenas et al.*, 2014].

In the present paper, this full θ distribution has therefore been modeled as the sum of two Gaussian functions at low ($\theta \approx \theta_{m1} \approx 15°$) and high ($\theta \approx \theta_{m2} \approx 70°$) obliquities, with a parameter Q^2 providing the relative amount of magnetic wave power at very oblique angles (see section 2). The latter important parameter Q depends on λ and geomagnetic activity, as represented here by the *Kp* index. The variation of Q as a function of *Kp* is presented in Figure 4. Cluster statistics are shown by filled cells of various colors, while modeled Q values are shown by contour lines. The numerical fit is again provided by a third-order polynomial depending on λ and *Kp*, separately in day and night sectors and for $4 < L < 5$ and $5 < L < 7$ domains

$$\log_{10} Q(\lambda, K_p) = \sum \sum b_{ij} (K_p)^j (\lambda[°]/10)^i \quad (6)$$

where $0 \le Kp < 8$. The corresponding coefficients are provided in Table 3.

Table 3. Values of the Coefficients b_{ij} for the Model of Chorus Wave Obliqueness Q (Day/Night Sectors; $4 < L < 5$ and $5 < L < 7$)

Sector	ij	0	1	2	3
			$4 < L < 5$		
Day	0	−2.96228	0.05432	0.01255	−0.00198
	1	−0.22490	2.56741	−0.47109	0.01404
	2	0.49580	−1.57164	0.26058	−0.00546
	3	−0.07438	0.23945	−0.03901	0.00069
Night	0	−2.36144	−0.67690	0.38151	−0.04328
	1	0.58891	0.83602	−0.22328	0.01204
	2	−0.20129	−0.41678	0.06725	0.00047
	3	0.05096	0.04697	−0.00506	−0.00055
			$5 < L < 7$		
Day	0	−2.33942	1.48424	−0.44211	0.02935
	1	3.97584	−2.60653	0.50009	−0.02391
	2	−2.00059	1.02028	−0.13731	0.00332
	3	0.27218	−0.11708	0.01089	0.00001
Night	0	−0.78880	−0.27695	0.14791	−0.04102
	1	0.64041	1.08776	−0.78908	0.13281
	2	−0.52973	−0.56092	0.45359	−0.07310
	3	0.09115	0.08602	−0.06941	0.01077

6. Model Incorporation Into Diffusion Rate Codes

To demonstrate the potential interest of the new wave model described in this paper, pitch angle diffusion coefficients of 100 keV electrons are calculated for the dayside lower L shell sector ($L = 5$, with a plasma frequency to electron equatorial gyrofrequency ratio ~4.5). The two different models of the wave amplitude and obliquity factor Q are used, with either a Kp or a Dst dependence on geomagnetic activity (the latter model is provided in Appendix A). The results are displayed in Figure 5. The difference between realistic Q values and $Q = 0$ (i.e., parallel wave approximation) is well seen. This difference is especially strong for small pitch angles where the presence of oblique waves results in a significant increase of the diffusion coefficients.

The increase of geomagnetic activity is seen to lead to a general growth of $D_{\alpha\alpha}$ (with Kp and $|Dst|$) related to the increase of the wave amplitude. This is a well-known effect, corresponding to more effective electron

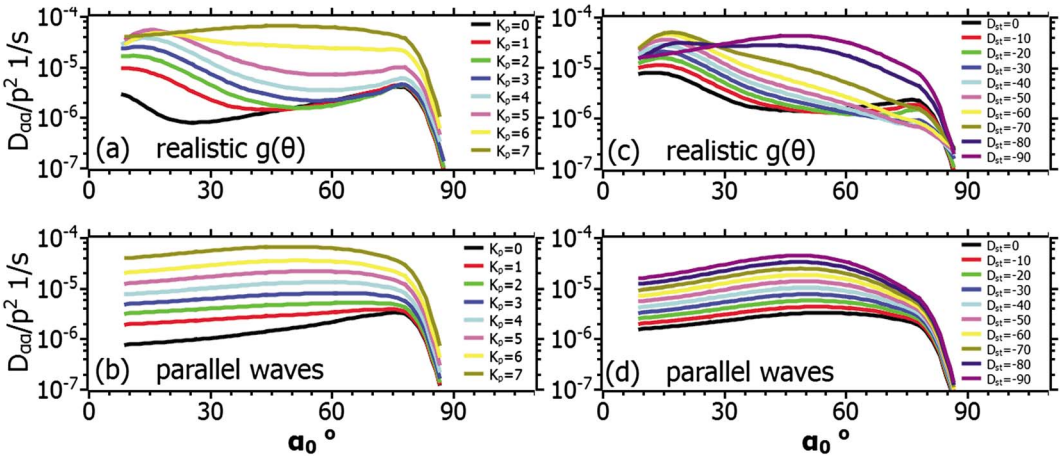

Figure 5. Bounce-averaged pitch angle diffusion coefficients for 100 keV electrons. Modeled variations of wave amplitude and Q factor with Kp and Dst are used. (a and c) Diffusion coefficients calculated for realistic distribution of θ angle (with approximated Q factor).(b and d) Results of calculations for parallel wave approximation $Q = 0$ (i.e., $g(\theta)$ distribution is the same as in *Glauert and Horne* [2005]).

scattering/acceleration during disturbed (high *Kp*) periods [e.g., *Horne et al.*, 2005b; *Thorne et al.*, 2013]. However, incorporating realistic θ distributions into the calculations of diffusion coefficients brings forth a new effect. At low geomagnetic activity, the high level of oblique waves produces a relative increase of electron scattering as compared with parallel waves alone, especially for small pitch angle electrons (compare $D_{\alpha\alpha}$ for $\alpha_0 < 30°$ for realistic $g(\theta)$ and for parallel waves in Figure 5). The increase of geomagnetic activity results in a redistribution of the wave θ angles (see Figure 4). The relative amount of oblique waves becomes smaller for higher geomagnetic activity, leading to a comparatively weaker scattering of small pitch angle electrons (compare results for parallel and oblique waves in Figure 5). It explains why there is no local maximum of $D_{\alpha\alpha}$ at small equatorial pitch angles α_0 for high *Kp* (or $|Dst|$) with the full wave model contrary to the low *Kp* range. Therefore, additionally to a general increase of the wave amplitude (and a corresponding global intensification of electron scattering) when *Kp* grows, the simultaneous evolution of the realistic $g(\theta)$ distribution with *Kp* modifies the profile of the pitch angle diffusion rate as a function of α_0. This new effect may in turn result in different pitch angle distribution shapes for the electrons [*Mourenas et al.*, 2015a].

Moreover, there is a clear difference between the $\langle D_{\alpha\alpha}\rangle$ profiles calculated with $Q(\lambda)$ and $B_w(\lambda)$ approximations as a function of *Kp* and *Dst*. The decrease of *Dst* first leads to a decrease of $\langle D_{\alpha\alpha}\rangle$ for high equatorial pitch angle electrons ($\alpha_0 \sim 75°$). For such a range of pitch angles, cyclotron resonance with the waves occurs at low latitudes. Thus, this decrease stems from an increase of the finite population of oblique waves near the equator in this intermediate *Dst* range [*Mourenas et al.*, 2014]. While the full range of *Q* variations with $Dst \in [-70, -10]$ nT roughly corresponds to the full range of *Q* variations for $Kp \in [1, 5]$, this effect also appears to be sensibly weaker for a *Q* variation modeled as a function of *Kp* instead of *Dst*: the increase of *Kp* does not result in a growth of the near-equatorial *Q* value as long as *Kp* remains < 4 (i.e., oblique waves remain elusive in this parameter domain). How can one explain such a discrepancy between results obtained for an increasing geomagnetic activity denoted by *Dst* and *Kp* indices?

Magnetospheric substorms, characterized by an increase of the *Kp* index, have long been associated with injections of hot electrons (a few keV to tens of keV) from the plasma sheet [*McIlwain*, 1974; *Sauvaud and Winckler*, 1980; *Delcourt et al.*, 1990]. Such hot electron injections are probably a key ingredient for the initial generation of chorus waves [*Meredith et al.*, 2001], necessary and maybe sufficient to jump-start the production of large increases of MeV electron flux in the outer belt even in the absence of a full-scale magnetic storm, i.e., even when *Dst* remains > -20 nT [*Meredith et al.*, 2003a; *Summers et al.*, 2004; *Miyoshi et al.*, 2007]. In this context, the difference in the wave-normal angular distributions of lower band chorus waves at latitudes $\lambda < 20°$ when considering $Kp < 3$ as compared with the range $Dst = 0$ to -50 nT could stem from the presence of substorms (with $Kp > 3$) during part of the periods such that $Dst = 0$ to -50 nT, while such substorms are likely absent (or very weak) when $Kp < 3$. Substorm-related injections of significant unstable populations of relatively hot electrons (~1–10 keV) could indeed be necessary for triggering the production of oblique waves at relatively low latitudes <20° [*Mourenas et al.*, 2015b]. An alternative possibility could be that the magnetic amplitude of parallel chorus waves generated during low *Kp* periods might be further reduced after their refraction along their propagation to higher latitudes [*Chen et al.*, 2013; *Breuillard et al.*, 2012], in such a way that these oblique waves could simply lie below the noise level of Cluster instruments. But the latter possibility looks rather unlikely in view of the presence of measured oblique waves at slightly higher latitudes in Cluster statistics at $Kp < 3$. We leave for future works a more detailed investigation of electron resonant scattering by whistler mode waves as described by the different proposed wave models.

7. Discussion and Conclusions

Wave-particle interactions are known to induce orders of magnitude variations of energetic electron fluxes in the radiation belts over timescales ranging from hours to weeks. Forecasting the evolution of the radiation belts is therefore a tremendous task. Nevertheless, it was marked by great advances in the past two decades, with the progressive incorporation of a greater number of relevant physical processes, more precise wave models, and the advent of refined ensemble Kalman filtering methods [e.g., see *Varotsou et al.*, 2005; *Shprits et al.*, 2008; *Su et al.*, 2011; *Horne et al.*, 2013; *Thorne et al.*, 2013; *Glauert et al.*, 2014; *Podladchikova et al.*, 2014]. In this context, an accurate determination of electron lifetimes and energization rates due to scattering by lower band chorus waves is a critical element for modeling and predicting the dynamics of the outer radiation belt. However, the latter requires a fair knowledge of the distributions of wave amplitudes and wave-normal angles as a function of many parameters, such as *L* shell, MLT, magnetic latitude λ, and geomagnetic activity.

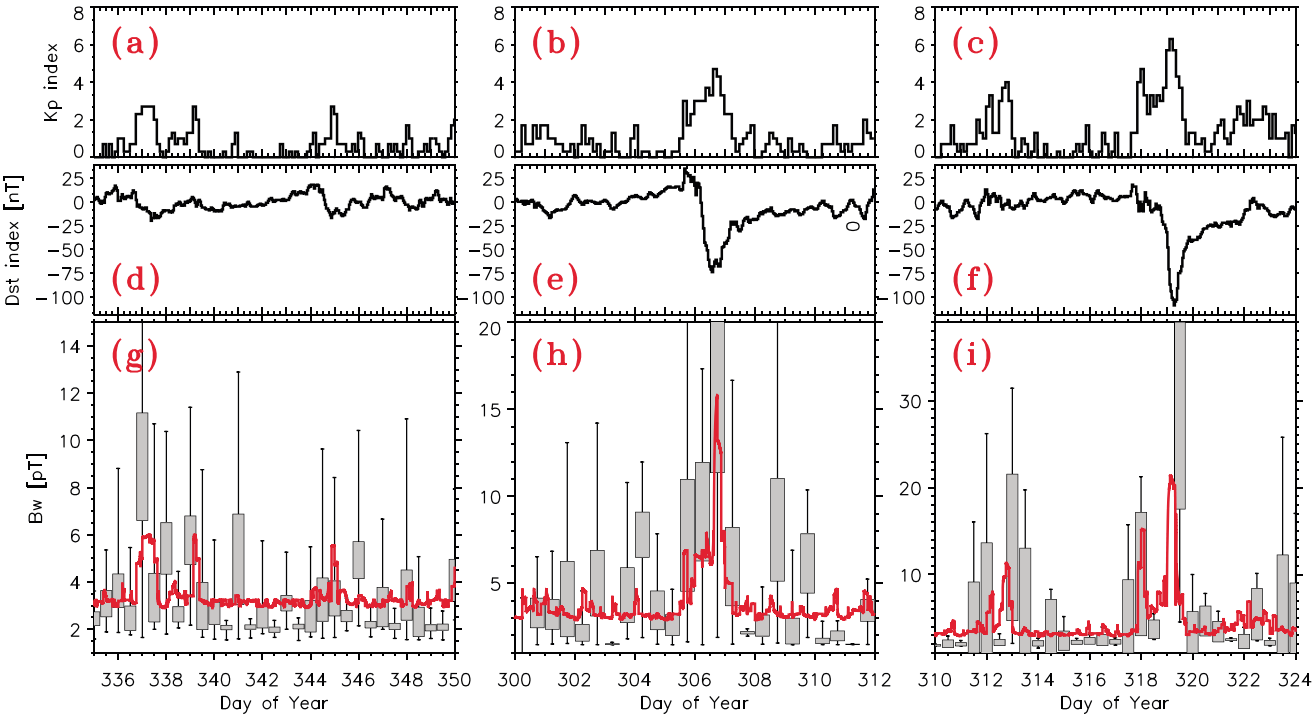

Figure 6. *Kp* and *Dst* indices dynamics and corresponding chorus waves amplitudes captured aboard the Van Allen Probes during three time intervals: (a, d, and g) quiet geomagnetic conditions of 1–14 December 2012, (b, e, and h) the intermediate geomagnetic storm of 26 October to 7 November 2012, and (c, f, and i) the geomagnetic storm of 5–19 November 2012. The averaged amplitudes obtained when crossing $L = 4.5 \pm 0.5$ are shown by grey rectangles indicating the confidence interval. Black error bars indicate the minimal and maximal values of observed wave amplitude. The wave amplitude modeled with equation (5) and coefficients from Table 2 is shown by red line.

The new lower band chorus wave parameterizations obtained in the present paper provide such an information on a statistical basis, building on the very large and comprehensive database of chorus amplitudes and wave normals obtained over 10 years by the Cluster spacecraft. The polynomial wave models provide the needed information as a function of geomagnetic activity, as described by either *Kp* or *Dst* indices. This could allow future detailed studies concerning the better relevance of one index as compared to the other in various space weather simulations or related to their likely complementarity in some parameter ranges as regards the information provided on the wave distribution.

Each wave model consists simply of two modeled distributions of lower band chorus wave RMS amplitude B_w and wave-normal angle θ provided as a function of *Kp* (or *Dst*) and magnetic latitude λ for day and night sectors of the outer radiation belt and for two ranges of *L* shell being covered: from 4 to 5 and from 5 to 7 (the latter for *Kp* only). Numerical calculations of wave particle scattering on the basis of the proposed wave models should hopefully allow an improved forecasting ability in the outer belt, while at the same time enabling the full numerical codes, for the first time, to study the different effects of *Kp* and *Dst* disturbances (roughly corresponding to substorms and storms) in shaping the Earth's outer radiation belt.

As a further and complementary validation, the dynamics of chorus wave amplitudes obtained with the *Kp* model at $4 < L < 5$ (using equation (5) and Table 2) is displayed in Figures 6g–6i over three different periods in October–December 2012, corresponding, respectively, to quiet geomagnetic conditions, a moderate geomagnetic storm with a minimum *Dst* of about −75 nT, and a larger geomagnetic storm with minimal *Dst* near −110 nT. Thanks to recent measurements by the two Van Allen Probes (see *Kletzing et al.* [2013] for details) (both of them crossed $L = 4$–5 four or six times each day at a latitude smaller than 20°), the variation of the measured wave amplitude can be compared with the wave amplitude variations obtained from the statistical wave model presented here. The period of October–December 2012 is chosen because it contained intervals of different geomagnetic activities, and the crossing of $L = 4.5$ by the Van Allen Probes spacecraft occurred from 2:00 to 10:00 MLT. Chorus wave amplitudes measured by the Van Allen Probes and averaged over 12 h time intervals are shown by grey rectangles indicating the averaging time interval (horizontal size)

and the confidence interval of chorus wave amplitude (vertical size), while minimal and maximal values of wave amplitude observed during each interval are indicated by error bars. One can note a good overall agreement between measured and modeled average amplitudes of chorus waves at $L \sim 4$–4.5, especially when taking into account both the uncertainties on the precise location of the magnetic equator and the observed amplitude fluctuations from one crossing to the next one. These examples demonstrate that the present wave model is able to roughly recover the full range of chorus wave power variations observed over the course of a geomagnetic storm in the domain $Kp \leq 7$, making it basically suitable for studying the outer radiation belt dynamics. However, some differences are also observed: the minimum amplitude level of Van Allen Probes data is ~1–2 pT lower than the modeled one. This can be explained by the higher sensitivity at low amplitudes provided by the Electric and Magnetic Field Instrument and Integrated Science (EMFISIS) [*Kletzing et al.*, 2013] than with Clusters STAFF-SA [*Cornilleau-Wehrlin et al.*, 2003] and by the different measurement regimes (averaging over 4 s interval for STAFF-SA and over 0.5 s for EMFISIS), leading to a higher variance of amplitude measurements when using EMFISIS. It is worth noting also that the modeled wave amplitudes tend to underestimate the observed chorus wave amplitudes during active times (as on days 337, 307, and 319) by factors ~1.3–1.5. This might be partly explained by the different regimes of measurements of STAFF-SA (averaging over 4 s) and EMFISIS (averaging over 0.5 s). Nevertheless, this underestimation remains limited as compared with the modeled large increases of the wave amplitude during these active periods by factors ~2 to 10 from the quiet time level. Another kind of differences can be noticed in Figures 6g–6i, corresponding to localized peaks of wave amplitude occurring during day 341 in Figure 6g and days 304 and 309 in Figure 6h. Such wave amplitude enhancements are observed without any significant increases of *Kp* (or |*Dst*|). To be able to reproduce such localized peaks, an even more complicated wave model would need to be developed, with a better resolution in MLT (< 2 h, requiring a much more detailed database) and based on some combination of geomagnetic indices and solar wind parameters.

Appendix A: Models of Wave Amplitude and Obliquity *Q* as a Function of *Dst*

Models of the RMS wave amplitude and θ distribution similar to the ones detailed in sections 4 and 5 can be provided as a function of the *Dst* index for outer belt chorus waves (here for $4 < L < 5$, where the lower limit for data consideration was taken as either $L = 4$ or plasmapause position if the latter is at larger L, see details in *Agapitov et al.* [2013]). For $4 < L < 5$, the coverage is sufficient for $Dst > -100$ nT in the day and night sectors. A gap in measurements occurs for $-175 < Dst < -100$ in the day sector with only some measurements in the MLT 6:00–12:00 sector for $-200 < Dst < -100$. In the night sector, measurements were present only for $-175 < Dst < -150$. For $Dst < -50$ nT, a sufficient coverage exists mainly for $|\lambda| < 35°$, while for -50 nT $< Dst < +25$ nT the coverage remains good as long as $|\lambda| < 45°$. The preceding values should be used as upper limits for λ when using the model.

For a given latitude, a good linear correlation can be found between the log value of the wave amplitude and *Dst* but with different amplitude levels at different latitudes (sometimes by an order of magnitude—not shown here but similar as in *Mourenas et al.* [2014]). This led us to compose the following linear model:

$$\log_{10} B_w(Dst) = A + BDst$$

where B_w and *Dst* are in nanotesla and coefficients A and B both depend on latitude. This dependence can be expressed as a polynom of order less than 4

$$A(\lambda) = a_0 + a_1\lambda + a_2\lambda^2 + a_3\lambda^3 + a_4\lambda^4$$

$$B(\lambda) = b_0 + b_1\lambda + b_2\lambda^2 + b_3\lambda^3 + b_4\lambda^4$$

with λ in degrees. The coefficients for the $A(\lambda)$ and $B(\lambda)$ fits are given in Table A1.

Table A1. Values of the Coefficients a_i and b_i for Day and Night Sectors for $4 < L < 5$ (*Dst* Model)

Sector	i	0	1	2	3	4
Day	a_i	−2.62	$4.86 \cdot 10^{-2}$	$2.00 \cdot 10^{-3}$	$-2.57 \cdot 10^{-4}$	$5.35 \cdot 10^{-6}$
	b_i	$-2.62 \cdot 10^{-3}$	$-6.05 \cdot 10^{-4}$	$-6.36 \cdot 10^{-6}$	$1.62 \cdot 10^{-6}$	$-2.27 \cdot 10^{-8}$
Night	a_i	−3.80	$4.84 \cdot 10^{-2}$	$-8.95 \cdot 10^{-4}$	$-11.1 \cdot 10^{-5}$	$2.80 \cdot 10^{-6}$
	b_i	$-8.62 \cdot 10^{-3}$	$2.34 \cdot 10^{-4}$	$2.50 \cdot 10^{-5}$	$-1.51 \cdot 10^{-6}$	$3.09 \cdot 10^{-8}$

Table A2. Values of the Coefficients b_{ij} for Day and Night Sectors for $4 < L < 5$ (*Dst* Model)

Sector	a	0	1	2	3
Day	b_{0j}	-2.70	$6.75 \cdot 10^{-3}$	$5.55 \cdot 10^{-4}$	$4.00 \cdot 10^{-6}$
	b_{1j}	$1.77 \cdot 10^{-1}$	$-8.65 \cdot 10^{-3}$	$-1.55 \cdot 10^{-4}$	$-3.50 \cdot 10^{-7}$
	b_{2j}	$-1.02 \cdot 10^{-2}$	$6.37 \cdot 10^{-4}$	$9.50 \cdot 10^{-6}$	$7.14 \cdot 10^{-9}$
	b_{3j}	$1.95 \cdot 10^{-4}$	$-1.19 \cdot 10^{-5}$	$-1.78 \cdot 10^{-7}$	$-1.20 \cdot 10^{-10}$
Night	b_{0j}	-3.15	$2.97 \cdot 10^{-3}$	$7.45 \cdot 10^{-4}$	$6.04 \cdot 10^{-6}$
	b_{1j}	$5.26 \cdot 10^{-2}$	$-7.61 \cdot 10^{-3}$	$-7.15 \cdot 10^{-5}$	$7.28 \cdot 10^{-9}$
	b_{2j}	$-1.32 \cdot 10^{-4}$	$3.88 \cdot 10^{-4}$	$5.83 \cdot 10^{-7}$	$-2.58 \cdot 10^{-8}$
	b_{3j}	$1.60 \cdot 10^{-5}$	$-4.65 \cdot 10^{-6}$	$2.57 \cdot 10^{-8}$	$6.10 \cdot 10^{-10}$

The model is provided in the form of the third degree polynomials as a function of λ and *Dst*

$$Q(\lambda, Dst) = \sum_{i=0}^{i=4} \sum_{i=0}^{i=4} b_{ij} \lambda^i Dst^j \tag{A1}$$

The coefficients are presented in Table A2.

Appendix B: Approximation of Wave Obliqueness for Measured B_w

If direct measurements of the RMS wave amplitudes *Bw* are already available and if one needs only a model of the θ distribution, the following approximation can be used. The parameter which determines the form of the distribution in such a case is the ratio of the number of oblique waves to the number of quasi-parallel waves $Q^2 = \sum_{\theta=60}^{\theta_{res}} N(\theta) / \sum_{\theta=0}^{45} N(\theta)$, which determines the relative levels of the two corresponding Gaussians.

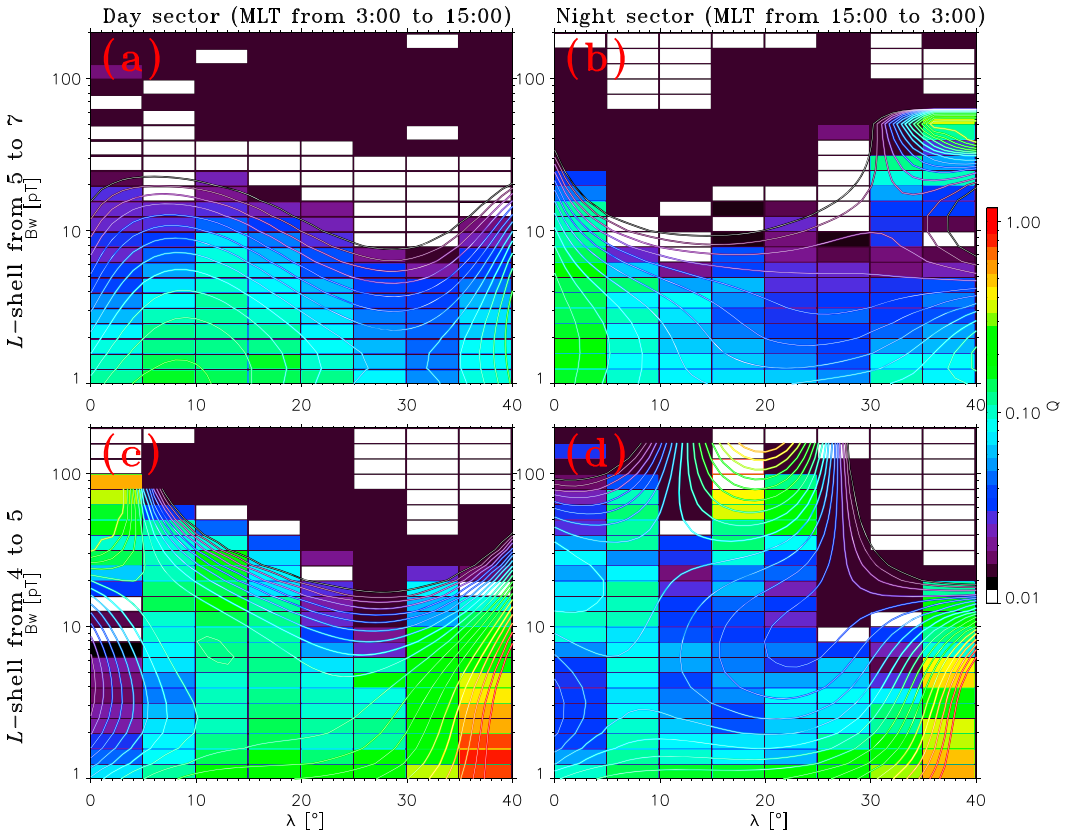

Figure A1. Distribution of the obliqueness parameter for chorus waves in the day and night sectors of the magnetosphere as a function of B_w for $4 < L < 5$.

Table B1. Values of the Coefficients α_{ij} for the Model of Chorus Wave Obliqueness on B_w

Sector	ij	0	1	2	3
			$4 < L < 5$		
Day	0	-1.31	-2.20	2.17	$-4.83 \cdot 10^{-1}$
	1	$9.06 \cdot 10^{-2}$	$7.88 \cdot 10^{-2}$	$2.10 \cdot 10^{-1}$	$-1.71 \cdot 10^{-1}$
	2	$-5.57 \cdot 10^{-3}$	$1.93 \cdot 10^{-3}$	$-2.76 \cdot 10^{-2}$	$1.61 \cdot 10^{-2}$
	3	$1.11 \cdot 10^{-4}$	$-6.52 \cdot 10^{-5}$	$5.42 \cdot 10^{-4}$	$-3.04 \cdot 10^{-4}$
Night	0	-1.12	-2.46	3.66	-1.36
	1	$4.52 \cdot 10^{-2}$	$2.06 \cdot 10^{-1}$	$-3.38 \cdot 10^{-1}$	$1.08 \cdot 10^{-1}$
	2	$-3.29 \cdot 10^{-3}$	$-1.37 \cdot 10^{-2}$	$1.45 \cdot 10^{-2}$	$-1.29 \cdot 10^{-3}$
	3	$7.92 \cdot 10^{-5}$	$2.53 \cdot 10^{-4}$	$-1.97 \cdot 10^{-4}$	$-4.37 \cdot 10^{-5}$
			$5 < L < 7$		
Day	0	-1.07	$-6.96 \cdot 10^{-1}$	$-2.29 \cdot 10^{-1}$	$7.17 \cdot 10^{-2}$
	1	$6.91 \cdot 10^{-2}$	$4.48 \cdot 10^{-2}$	$1.35 \cdot 10^{-1}$	$-1.31 \cdot 10^{-1}$
	2	$-5.81 \cdot 10^{-3}$	$1.05 \cdot 10^{-3}$	$-1.70 \cdot 10^{-2}$	$1.22 \cdot 10^{-2}$
	3	$1.05 \cdot 10^{-4}$	$-3.92 \cdot 10^{-5}$	$3.42 \cdot 10^{-4}$	$-2.32 \cdot 10^{-4}$
Night	0	$-8.91 \cdot 10^{-1}$	$-2.93 \cdot 10^{-2}$	$1.75 \cdot 10^{-1}$	$-4.44 \cdot 10^{-1}$
	1	$-5.55 \cdot 10^{-2}$	$1.21 \cdot 10^{-1}$	$-2.25 \cdot 10^{-1}$	$-1.25 \cdot 10^{-2}$
	2	$2.07 \cdot 10^{-3}$	$-1.55 \cdot 10^{-2}$	$2.84 \cdot 10^{-2}$	$-5.91 \cdot 10^{-3}$
	3	$-2.00 \cdot 10^{-5}$	$3.41 \cdot 10^{-4}$	$-6.78 \cdot 10^{-4}$	$2.19 \cdot 10^{-4}$

The dependence of wave obliqueness on wave amplitude (high B_w chorus waves are mainly field aligned while low amplitude waves become more oblique) led to the chosen format of the proposed model in the form of a double polynomial dependence on B_w (in pico)

$$\log_{10} Q^2(B_w[pT], \lambda) = \sum_{i=0}^{n} \sum_{j=0}^{n} \alpha_{ij} \lambda^j (\log_{10} B_w[pT])^i, \tag{B1}$$

where λ is in degrees. However, the sparse data in some parameter zones do not allow to use only the simple polynomial fit above. An additional refinement is performed on the nightside at $L = 5–7$ and latitude $\lambda > 30°$, where the maximum level of obliquity is limited by using $Q = \min(Q, 0.35)$. Also, one should note that the model works reliably only up to $B_w < 65$ pT in this domain. Similarly, on the dayside at $L = 4–5$ and $\lambda < 5°$, an obliquity limiter $Q = \min(Q, 0.3)$ is used to better reproduce the present Cluster data — in agreement also with previous THEMIS statistics indicating that lower band chorus waves with $B_w > 50$ pT are mainly quasi-parallel near the equator [*Li et al.*, 2011]. Both experimental data and contour levels of approximations are shown in Figure A1.

For both dependencies (small and large L shells), third-order polynomials were selected (coefficients are listed in Table B1). Note that the black and white levels in Figure A1 correspond to very rare oblique waves, which are not observed on a regular basis. Since our approximate statistical wave model is intended to represent the average waves encountered by trapped electrons over limited time periods (days to weeks), such extremely rare oblique wave occurrences should be set to zero (or any negligible value) in the average wave model. Thus, the final expression of the average wave obliqueness Q_{av} as a function of wave amplitude and latitude can be written as

$$Q_{av}^2 \sim Q^2 H(Q^2 - 0.014) \tag{B2}$$

where H denotes the Heaviside function (whose value is 0 for negative argument and 1 for positive argument). A rough but similar model obtained over $L \sim 4–6$ mainly on the night sector has been used recently in the work by *Li et al.* [2014] to compare 30–100 keV electron pitch angle scattering losses induced by realistic (oblique and parallel) waves and parallel-only waves, showing a reasonable agreement with satellite observations during Polar Operational Environmental Satellite-Van Allen Probes conjunction events.

The good overall agreement obtained between the wave model distributions and the experimental data makes this wave model particularly suitable for numerical calculations of particle scattering in space weather

codes aiming at obtaining typical (and sufficiently accurate) electron flux evolutions in the considered geomagnetic activity ranges. Furthermore, its relatively simple analytical form may provide a unique opportunity of using the proposed statistical model in simplified analytical investigations of the effects of *Dst* and *Kp* variations on the outer radiation belt.

Acknowledgments
The work by O.A. and F.M. was performed under JHU/APL contract 922613 (RBSP-EFW) and NASA NNX09AE41G-1/14 contract. The work of A.A.V. was supported by the grant MK-1781.2014.2. All the data used in the paper were obtained from Cluster Active Archive http://caa.estec.esa.int/ (STAFF-SA, FGM, particle data) and http://omniweb.gsfc.nasa.gov/ (geomagnetic indices data).

References

Agapitov, O., V. Krasnoselskikh, Y. Zaliznyak, V. Angelopoulos, O. Le Contel, and G. Rolland (2010), Chorus source region localization in the Earth's outer magnetosphere using THEMIS measurements, *Ann. Geophys.*, *28*, 1377–1386.

Agapitov, O., V. Krasnoselskikh, T. Dudok de Wit, Y. Khotyaintsev, J. S. Pickett, O. Santolík, and G. Rolland (2011a), Multispacecraft observations of chorus emissions as a tool for the plasma density fluctuations' remote sensing, *J. Geophys. Res.*, *116*, A09222, doi:10.1029/2011JA016540.

Agapitov, O., V. Krasnoselskikh, Y. V. Khotyaintsev, and G. Rolland (2011b), A statistical study of the propagation characteristics of whistler waves observed by Cluster, *Geophys. Res. Lett.*, *382*, L20103, doi:10.1029/2011GL049597.

Agapitov, O., V. Krasnoselskikh, Y. Zaliznyak, V. Angelopoulos, O. Le Contel, and G. Rolland (2011c), Observations and modeling of forward and reflected chorus waves captured by THEMIS, *Ann. Geophys.*, *29*, 541–550, doi:10.5194/angeo-29-541-2011.

Agapitov, O., V. Krasnoselskikh, Y. V. Khotyaintsev, and G. Rolland (2012), Correction to "A statistical study of the propagation characteristics of whistler waves observed by Cluster", *Geophys. Res. Lett.*, *39*, L24102, doi:10.1029/2012GL054320.

Agapitov, O., A. Artemyev, V. Krasnoselskikh, Y. V. Khotyaintsev, D. Mourenas, H. Breuillard, M. Balikhin, and G. Rolland (2013), Statistics of whistler mode waves in the outer radiation belt: Cluster STAFF-SA measurements, *J. Geophys. Res. Space Physics*, *118*, 3407–3420, doi:10.1002/jgra.50312.

Albert, J. M. (2007), Simple approximations of quasi-linear diffusion coefficients, *J. Geophys. Res.*, *112*, A12202, doi:10.1029/2007JA012551.

Albert, J. M. (2008), Efficient approximations of quasi-linear diffusion coefficients in the radiation belts, *J. Geophys. Res.*, *113*, A06208, doi:10.1029/2007JA012936.

Albert, J. M. (2012), Dependence of quasi-linear diffusion coefficients on wave parameters, *J. Geophys. Res.*, *117*, A09224, doi:10.1029/2012JA017718.

André, R., F. Lefeuvre, F. Simonet, and U. S. Inan (2002), A first approach to model the low-frequency wave activity in the plasmasphere, *Ann. Geophys.*, *20*, 981–996, doi:10.5194/angeo-20-981-2002.

Artemyev, A., O. Agapitov, H. Breuillard, V. Krasnoselskikh, and G. Rolland (2012a), Electron pitch-angle diffusion in radiation belts: The effects of whistler wave oblique propagation, *Geophys. Res. Lett.*, *39*, L08105, doi:10.1029/2012GL051393.

Artemyev, A., O. Agapitov, V. Krasnoselskikh, H. Breuillard, and G. Rolland (2012b), Statistical model of electron pitch-angle diffusion in the outer radiation belt, *J. Geophys. Res.*, *117*, A08219, doi:10.1029/2012JA017826.

Artemyev, A. V., O. V. Agapitov, D. Mourenas, V. Krasnoselskikh, and L. M. Zelenyi (2013a), Storm-induced energization of radiation belt electrons: Effect of wave obliquity, *Geophys. Res. Lett.*, *40*, 4138–4143, doi:10.1002/grl.50837.

Artemyev, A. V., D. Mourenas, O. V. Agapitov, and V. V. Krasnoselskikh (2013b), Parametric validations of analytical lifetime estimates for radiation belt electron diffusion by whistler waves, *Ann. Geophys.*, *31*, 599–624, doi:10.5194/angeo-31-599-2013.

Balikhin, M. A., R. J. Boynton, S. N. Walker, J. E. Borovsky, S. A. Billings, and H. L. Wei (2011), Using the NARMAX approach to model the evolution of energetic electrons fluxes at geostationary orbit, *Geophys. Res. Lett.*, *38*, L18105, doi:10.1029/2011GL048980.

Bortnik, J., U. S. Inan, and T. F. Bell (2006), Landau damping and resultant unidirectional propagation of chorus waves, *Geophys. Res. Lett.*, *33*, L03102, doi:10.1029/2005GL024553.

Boynton, R. J., M. A. Balikhin, S. A. Billings, G. D. Reeves, N. Ganushkina, M. Gedalin, O. A. Amariutei, J. E. Borovsky, and S. N. Walker (2013), The analysis of electron fluxes at geosynchronous orbit employing a NARMAX approach, *J. Geophys. Res. Space Physics*, *118*, 1500–1513, doi:10.1002/jgra.50192.

Breuillard, H., Y. Zaliznyak, V. Krasnoselskikh, O. Agapitov, A. Artemyev, and G. Rolland (2012), Chorus wave-normal statistics in the Earth's radiation belts from ray tracing technique, *Ann. Geophys.*, *30*, 1223–1233, doi:10.5194/angeo-30-1223-2012.

Breuillard, H., et al. (2015), Field-aligned chorus wave spectral power in Earth's outer radiation belt, *Ann. Geophys.*, *33*(5), 583–597, doi:10.5194/angeo-33-583-2015.

Bunch, N. L., M. Spasojevic, and Y. Y. Shprits (2012), Off-equatorial chorus occurrence and wave amplitude distributions as observed by the Polar Plasma Wave Instrument, *J. Geophys. Res.*, *117*, A04205, doi:10.1029/2011JA017228.

Bunch, N. L., M. Spasojevic, Y. Y. Shprits, X. Gu, and F. Foust (2013), The spectral extent of chorus in the off-equatorial magnetosphere, *J. Geophys. Res. Space Physics*, *118*, 1700–1705, doi:10.1029/2012JA018182.

Burtis, W. J., and R. A. Helliwell (1976), Magnetospheric chorus—Occurrence patterns and normalized frequency, *Planet. Space Sci.*, *24*, 1007–1024, doi:10.1016/0032-0633(76)90119-7.

Burton, R. K., and R. E. Holzer (1974), The origin and propagation of chorus in the outer magnetosphere, *J. Geophys. Res.*, *79*, 1014–1023, doi:10.1029/JA079i007p01014.

Chen, L., R. M. Thorne, W. Li, and J. Bortnik (2013), Modeling the wave normal distribution of chorus waves, *J. Geophys. Res. Space Physics*, *118*, 1074–1088, doi:10.1029/2012JA018343.

Cornilleau-Wehrlin, N., et al. (2003), First results obtained by the Cluster STAFF experiment, *Ann. Geophys.*, *21*, 437–456, doi:10.5194/angeo-21-437-2003.

Cully, C. M., J. W. Bonnell, and R. E. Ergun (2008), THEMIS observations of long-lived regions of large-amplitude whistler waves in the inner magnetosphere, *Geophys. Res. Lett.*, *35*, L17S16, doi:10.1029/2008GL033643.

Delcourt, D. C., A. Pedersen, and J. A. Sauvaud (1990), Dynamics of single-particle orbits during substorm expansion phase, *J. Geophys. Res.*, *95*, 20,853–20,865, doi:10.1029/JA095iA12p20853.

Denton, R. E., et al. (2006), Distribution of density along magnetospheric field lines, *J. Geophys. Res*, *111*, A04213, doi:10.1029/2005JA011414.

Doe, R. A., M. B. Moldwin, and M. Mendillo (1992), Plasmapause morphology determined from an empirical ionospheric convection model, *J. Geophys. Res.*, *97*, A00F02, doi:10.1029/91JA01649.

Gendrin, R. (1961), Le guidage des whistlers par le champ magnetique, *Planet. Space Sci.*, *5*, 274–278, doi:10.1016/0032-0633(61)90096-4.

Glauert, S. A., and R. B. Horne (2005), Calculation of pitch angle and energy diffusion coefficients with the PADIE code, *J. Geophys. Res.*, *110*, A04206, doi:10.1029/2004JA010851.

Glauert, S. A., R. B. Horne, and N. P. Meredith (2014), Three-dimensional electron radiation belt simulations using the BAS Radiation Belt Model with new diffusion models for chorus, plasmaspheric hiss, and lightning-generated whistlers, *J. Geophys. Res. Space Physics*, *119*, 268–289, doi:10.1002/2013JA019281.

Goldstein, B. E., and B. T. Tsurutani (1984), Wave normal directions of chorus near the equatorial source region, *J. Geophys. Res.*, *89*, 2789–2810, doi:10.1029/JA089iA05p02789.
Gonzalez, W. D., J. A. Joselyn, Y. Kamide, H. W. Kroehl, G. Rostoker, B. T. Tsurutani, and V. M. Vasyliunas (1994), What is a geomagnetic storm?, *J. Geophys. Res.*, *99*, 5771–5792, doi:10.1029/93JA02867.
Gurnett, D. A., and U. S. Inan (1988), Plasma wave observations with the Dynamics Explorer 1 spacecraft, *Rev. Geophys.*, *26*, 285–316, doi:10.1029/RG026i002p00285.
Gustafsson, G., et al. (2001), First results of electric field and density observations by Cluster EFW based on initial months of operation, *Ann. Geophys.*, *19*, 1219–1240, doi:10.5194/angeo-19-1219-2001.
Haque, N., M. Spasojevic, O. Santolík, and U. S. Inan (2010), Wave normal angles of magnetospheric chorus emissions observed on the Polar spacecraft, *J. Geophys. Res.*, *115*, A00F07, doi:10.1029/2009JA014717.
Hayakawa, M., Y. Yamanaka, M. Parrot, and F. Lefeuvre (1984), The wave normals of magnetospheric chorus emissions observed on board GEOS 2, *J. Geophys. Res.*, *89*, 2811–2821, doi:10.1029/JA089iA05p02811.
Helliwell, R. A. (1965), *Whistlers and Related Ionospheric Phenomena*, Stanford Univ. Press, Stanford, Calif.
Horne, R. B., et al. (2005a), Wave acceleration of electrons in the Van Allen radiation belts, *Nature*, *437*, 227–230, doi:10.1038/nature03939.
Horne, R. B., R. M. Thorne, S. A. Glauert, J. M. Albert, N. P. Meredith, and R. R. Anderson (2005b), Timescale for radiation belt electron acceleration by whistler mode chorus waves, *J. Geophys. Res.*, *110*, A03225, doi:10.1029/2004JA010811.
Horne, R. B., S. A. Glauert, N. P. Meredith, D. Boscher, V. Maget, D. Heynderickx, and D. Pitchford (2013), Space weather impacts on satellites and forecasting the Earth's electron radiation belts with SPACECAST, *Space Weather*, *11*, 169–186, doi:10.1002/swe.20023.
Huttunen, K. E. J., H. E. J. Koskinen, and R. Schwenn (2002), Variability of magnetospheric storms driven by different solar wind perturbations, *J. Geophys. Res.*, *107*, 1121, doi:10.1029/2001JA900171.
Kellerman, A. C., Y. Y. Shprits, and D. L. Turner (2013), A Geosynchronous Radiation-belt Electron Empirical Prediction (GREEP) model, *Space Weather*, *11*, 463–475, doi:10.1002/swe.20074.
Kennel, C. F., and H. E. Petschek (1966), Limit on stably trapped particle fluxes, *J. Geophys. Res.*, *71*, 1–28.
Kim, K.-C., Y. Shprits, J. Lee, and J. Hwang (2013), Empirically modeled global distribution of magnetospheric chorus amplitude using an artificial neural network, *J. Geophys. Res. Space Physics*, *118*, 6243–6253, doi:10.1002/jgra.50595.
Kletzing, C. A., et al. (2013), The Electric and Magnetic Field Instrument Suite and Integrated Science (EMFISIS) on RBSP, *Space Sci. Rev.*, *179*, 127–181, doi:10.1007/s11214-013-9993-6.
Koons, H. C., and J. L. Roeder (1990), A survey of equatorial magnetospheric wave activity between 5 and 8 R(E), *Planet. Space Sci.*, *38*, 1335–1341, doi:10.1016/0032-0633(90)90136-E.
Lauben, D. S., U. S. Inan, T. F. Bell, and D. A. Gurnett (2002), Source characteristics of ELF/VLF chorus, *J. Geophys. Res.*, *107*, 1429, doi:10.1029/2000JA003019.
Li, W., J. Bortnik, R. M. Thorne, and V. Angelopoulos (2011), Global distribution of wave amplitudes and wave normal angles of chorus waves using THEMIS wave observations, *J. Geophys. Res.*, *116*, A12205, doi:10.1029/2011JA017035.
Li, W., et al. (2013a), An unusual enhancement of low-frequency plasmaspheric hiss in the outer plasmasphere associated with substorm-injected electrons, *Geophys. Res. Lett.*, *40*, 3798–3803, doi:10.1002/grl.50787.
Li, W., et al. (2013b), Characteristics of the Poynting flux and wave normal vectors of whistler-mode waves observed on THEMIS, *J. Geophys. Res. Space Physics*, *118*, 1461–1471, doi:10.1002/jgra.50176.
Li, W., et al. (2014), Evidence of stronger pitch angle scattering loss caused by oblique whistler-mode waves as compared with quasi-parallel waves, *Geophys. Res. Lett.*, *41*, 6063–6070, doi:10.1002/2014GL061260.
Lyons, L. R., and D. J. Williams (1984), *Quantitative Aspects of Magnetospheric Physics*, Springer, Netherlands.
Mayaud, P. N. (1980), *Derivation, Meaning, and Use of Geomagnetic Indices*, vol. 22, 607 pp., AGU, Washington, D. C.
McIlwain, C. E. (1974), Substorm injection boundaries, in *Magnetospheric Physics*, edited by B. M. McCormac, pp. 143–154, D. Reidel, Norwell, Mass.
Meredith, N. P., R. B. Horne, and R. R. Anderson (2001), Substorm dependence of chorus amplitudes: Implications for the acceleration of electrons to relativistic energies, *J. Geophys. Res.*, *106*, 13,165–13,178, doi:10.1029/2000JA900156.
Meredith, N. P., M. Cain, R. B. Horne, R. M. Thorne, D. Summers, and R. R. Anderson (2003a), Evidence for chorus-driven electron acceleration to relativistic energies from a survey of geomagnetically disturbed periods, *J. Geophys. Res.*, *108*, 1248, doi:10.1029/2002JA009764.
Meredith, N. P., R. B. Horne, R. M. Thorne, and R. R. Anderson (2003b), Favored regions for chorus-driven electron acceleration to relativistic energies in the Earth's outer radiation belt, *Geophys. Res. Lett.*, *30*(16), 1871, doi:10.1029/2003GL017698.
Meredith, N. P., R. B. Horne, R. M. Thorne, D. Summers, and R. R. Anderson (2004), Substorm dependence of plasmaspheric hiss, *J. Geophys. Res.*, *109*, A06209, doi:10.1029/2004JA010387.
Meredith, N. P., R. B. Horne, A. Sicard-Piet, D. Boscher, K. H. Yearby, W. Li, and R. M. Thorne (2012), Global model of lower band and upper band chorus from multiple satellite observations, *J. Geophys. Res.*, *117*, A10225, doi:10.1029/2012JA017978.
Meredith, N. P., R. B. Horne, T. Kersten, B. J. Fraser, and R. S. Grew (2014), Global morphology and spectral properties of EMIC waves derived from CRRES observations, *J. Geophys. Res.*, *119*, A10225, doi:10.1002/2014JA020064.
Miyoshi, Y., A. Morioka, R. Kataoka, Y. Kasahara, and T. Mukai (2007), Evolution of the outer radiation belt during the November 1993 storms driven by corotating interaction regions, *J. Geophys. Res.*, *112*, A05210, doi:10.1029/2006JA012148.
Mourenas, D., and J.-F. Ripoll (2012), Analytical estimates of quasi-linear diffusion coefficients and electron lifetimes in the inner radiation belt, *J. Geophys. Res.*, *117*, A01204, doi:10.1029/2011JA016985.
Mourenas, D., A. V. Artemyev, J.-F. Ripoll, O. V. Agapitov, and V. V. Krasnoselskikh (2012), Timescales for electron quasi-linear diffusion by parallel and oblique lower-band chorus waves, *J. Geophys. Res.*, *117*, A06234, doi:10.1029/2012JA017717.
Mourenas, D., A. V. Artemyev, O. V. Agapitov, and V. Krasnoselskikh (2013), Analytical estimates of electron quasi-linear diffusion by fast magnetosonic waves, *J. Geophys. Res. Space Physics*, *118*, 3096–3112, doi:10.1002/jgra.50349.
Mourenas, D., A. V. Artemyev, O. V. Agapitov, and V. Krasnoselskikh (2014), Consequences of geomagnetic activity on energization and loss of radiation belt electrons by oblique chorus waves, *J. Geophys. Res. Space Physics*, *119*, 2775–2796, doi:10.1002/2013JA019674.
Mourenas, D., A. V. Artemyev, O. V. Agapitov, V. Krasnoselskikh, and W. Li (2015a), Approximate analytical solutions for the trapped electron distribution due to quasi-linear diffusion by whistler-mode waves, *J. Geophys. Res. Space Physics*, *119*, 9962–9977, doi:10.1002/2014JA020443.
Mourenas, D., A. V. Artemyev, O. V. Agapitov, V. Krasnoselskikh, and F. Mozer (2015b), Very oblique whistler generation by low-energy electron streams, *J. Geophys. Res. Space Physics*, *120*, 3665–3683, doi:10.1002/2015JA021135.
Ni, B., R. M. Thorne, N. P. Meredith, Y. Y. Shprits, and R. B. Horne (2011), Diffuse auroral scattering by whistler mode chorus waves: Dependence on wave normal angle distribution, *J. Geophys. Res.*, *116*, A10207, doi:10.1029/2011JA016517.

Ni, B., J. Bortnik, R. M. Thorne, Q. Ma, and L. Chen (2013), Resonant scattering and resultant pitch angle evolution of relativistic electrons by plasmaspheric hiss, *J. Geophys. Res. Space Physics*, *118*, 7740–7751, doi:10.1002/2013JA019260.
Nikolaeva, N. S., Y. I. Yermolaev, and I. G. Lodkina (2011), Dependence of geomagnetic activity during magnetic storms on the solar wind parameters for different types of streams, *Geomagn. Aeron.*, *51*, 49–65, doi:10.1134/S0016793211010099.
Nikolaeva, N. S., Y. I. Yermolaev, and I. G. Lodkina (2013), Modeling the time behavior of the Dst index during the main phase of magnetic storms generated by various types of solar wind, *Cosmic Res.*, *51*, 401–412, doi:10.1134/S0010952513060038.
Ozhogin, P., J. Tu, P. Song, and B. W. Reinisch (2012), Field-aligned distribution of the plasmaspheric electron density: An empirical model derived from the IMAGE RPI measurements, *J. Geophys. Res.*, *117*, A06225, doi:10.1029/2011JA017330.
Parrot, M., O. Santolík, N. Cornilleau-Wehrlin, M. Maksimovic, and C. Harvey (2003), Magnetospherically reflected chorus waves revealed by ray tracing with CLUSTER data, *Ann. Geophys.*, *21*, 1111–1120, doi:10.5194/angeo-21-1111-2003.
Podladchikova, T. V., Y. Y. Shprits, D. Kondrashov, and A. C. Kellerman (2014), Noise statistics identification for Kalman filtering of the electron radiation belt observations I: Model errors, *J. Geophys. Res. Space Physics*, *119*, 5700–5724, doi:10.1002/2014JA019897.
Pokhotelov, D., F. Lefeuvre, R. B. Horne, and N. Cornilleau-Wehrlin (2008), Survey of ELF-VLF plasma waves in outer radiation belt observed by Cluster STAFF-SA experiment, *Ann. Geophys.*, *26*, 3269–3277, doi:10.5194/angeo-26-3269-2008.
Santolík, O., E. Macúšová, I. Kolmašová, N. Cornilleau-Wehrlin, and Y. Conchy (2014), Propagation of lower-band whistler-mode waves in the outer Van Allen belt: Systematic analysis of 11 years of multi-component data from the Cluster spacecraft, *Geophys. Res. Lett.*, *41*, 2729–2737, doi:10.1002/2014GL059815.
Sauvaud, J.-A., and J. R. Winckler (1980), Dynamics of plasma, energetic particles, and fields near synchronous orbit in the nighttime sector during magnetospheric substorms, *J. Geophys. Res.*, *85*, 2043–2056, doi:10.1029/JA085iA05p02043.
Sazhin, S. S., and M. Hayakawa (1992), Magnetospheric chorus emissions—A review, *Planet. Space Sci.*, *40*, 681–697, doi:10.1016/0032-0633(92)90009-D.
Sheeley, B. W., M. B. Moldwin, H. K. Rassoul, and R. R. Anderson (2001), An empirical plasmasphere and trough density model: CRRES observations, *J. Geophys. Res.*, *106*, 25,631–25,642, doi:10.1029/2000JA000286.
Shklyar, D., J. Chum, and F. Jirícek (2004), Characteristic properties of Nu whistlers as inferred from observations and numerical modelling, *Ann. Geophys.*, *22*, 3589–3606, doi:10.5194/angeo-22-3589-2004.
Shprits, Y. Y., and B. Ni (2009), Dependence of the quasi-linear scattering rates on the wave normal distribution of chorus waves, *J. Geophys. Res.*, *114*, A11205, doi:10.1029/2009JA014223.
Shprits, Y. Y., R. M. Thorne, R. B. Horne, and D. Summers (2006), Bounce-averaged diffusion coefficients for field-aligned chorus waves, *J. Geophys. Res.*, *111*, A10225, doi:10.1029/2006JA011725.
Shprits, Y. Y., N. P. Meredith, and R. M. Thorne (2007), Parameterization of radiation belt electron loss timescales due to interactions with chorus waves, *Geophys. Res. Lett.*, *34*, L11110, doi:10.1029/2006GL029050.
Shprits, Y. Y., D. A. Subbotin, N. P. Meredith, and S. R. Elkington (2008), Review of modeling of losses and sources of relativistic electrons in the outer radiation belt II: Local acceleration and loss, *J. Atmos. Sol. Terr. Phys.*, *70*, 1694–1713, doi:10.1016/j.jastp.2008.06.014.
Spasojevic, M., and Y. Y. Shprits (2013), Chorus functional dependencies derived from CRRES data, *Geophys. Res. Lett.*, *40*, 3793–3797, doi:10.1002/grl.50755.
Su, Z., F. Xiao, H. Zheng, and S. Wang (2011), CRRES observation and STEERB simulation of the 9 October 1990 electron radiation belt dropout event, *Geophys. Res. Lett.*, *38*, L06106, doi:10.1029/2011GL046873.
Summers, D. (2005), Quasi-linear diffusion coefficients for field-aligned electromagnetic waves with applications to the magnetosphere, *J. Geophys. Res.*, *110*, A08213, doi:10.1029/2005JA011159.
Summers, D., C. Ma, N. P. Meredith, R. B. Horne, R. M. Thorne, and R. R. Anderson (2004), Modeling outer-zone relativistic electron response to whistler-mode chorus activity during substorms, *J. Atmos. Sol. Terr. Phys.*, *66*, 133–146, doi:10.1016/j.jastp.2003.09.013.
Summers, D., B. Ni, and N. P. Meredith (2007), Timescales for radiation belt electron acceleration and loss due to resonant wave-particle interactions: 1. Theory, *J. Geophys. Res.*, *112*, A04206, doi:10.1029/2006JA011801.
Thorne, R. M., et al. (2013), Rapid local acceleration of relativistic radiation-belt electrons by magnetospheric chorus, *Nature*, *504*, 411–414, doi:10.1038/nature12889.
Trakhtengerts, V. Y. (1966), Stationary states of the Earth's outer radiation zone, *Geomagn. Aeron.*, *6*, 827–836.
Tsurutani, B. T., and E. J. Smith (1974), Postmidnight chorus: A substorm phenomenon, *J. Geophys. Res.*, *79*, 118–127, doi:10.1029/JA079i001p00118.
Tsyganenko, N. A., H. J. Singer, and J. C. Kasper (2003), Storm-time distortion of the inner magnetosphere: How severe can it get?, *J. Geophys. Res.*, *108*, 1209, doi:10.1029/2002JA009808.
Varotsou, A., D. Boscher, S. Bourdarie, R. B. Horne, S. A. Glauert, and N. P. Meredith (2005), Simulation of the outer radiation belt electrons near geosynchronous orbit including both radial diffusion and resonant interaction with Whistler-mode chorus waves, *Geophys. Res. Lett.*, *32*, L19106, doi:10.1029/2005GL023282.
Yermolaev, Y. I., and M. Y. Yermolaev (2003), Statistical relationships between solar, interplanetary, and geomagnetic disturbances, 1976–2000: 3, *Cosmic Res.*, *41*, 539–549, doi:10.1023/B:COSM.0000007952.09069.b8.

Erratum

In the originally published version of this article, Tables 2 and 3 contained incorrect entries. In addition, equations (5) and (6) were missing the sign LOG10. These errors have been corrected, and this version may be considered the authoritative version of record.